Cross-Component Energy Transfer in Superfluid Helium-4

Piotr Z. Stasiak[1] · Andrew W. Baggaley[1] · Giorgio Krstulovic[2] ·
Carlo F. Barenghi[1] · Luca Galantucci[1,3]

Abstract

The reciprocal energy and enstrophy transfers between normal fluid and superfluid components dictate the overall dynamics of superfluid ^{4}He including the generation, evolution and coupling of coherent structures, the distribution of energy among lengthscales, and the decay of turbulence. To better understand the essential ingredients of this interaction, we employ a numerical two-way model which self-consistently accounts for the back-reaction of the superfluid vortex lines onto the normal fluid. Here we focus on a prototypical laminar (non-turbulent) vortex configuration which is simple enough to clearly relate the geometry of the vortex line to energy injection and dissipation to/from the normal fluid: a Kelvin wave excitation on two vortex anti-vortex pairs evolving in (a) an initially quiescent normal fluid, and (b) an imposed counterflow. In (a), the superfluid injects energy and vorticity in the normal fluid. In (b), the superfluid gains energy from the normal fluid via the Donnelly–Glaberson instability.

Keywords Superfluid · ^{4}He · Thermal counterflow · Energy transfer · Fully-coupled dynamics

1 Introduction

The turbulent flow of helium II (the low temperature phase of liquid ^{4}He) consists of a disordered tangle of interacting superfluid vortex lines which move in a thermal background of elementary excitations [1–4]. The vortex lines are topological defects of the superfluid component [5–7], which is associated with the ground state, while the thermal excitations constitute a viscous fluid (the normal fluid component). According to the two-fluid theory [8, 9], normal fluid and superfluid are inseparable, penetrate each other and comprise of independent density and velocity fields. Importantly, since the vortex lines act as scattering centres for the elementary excitations, normal fluid and superfluid are dynamically coupled [7]. This interaction, called the mutual friction force, transfers kinetic

---

Extended author information available on the last page of the article
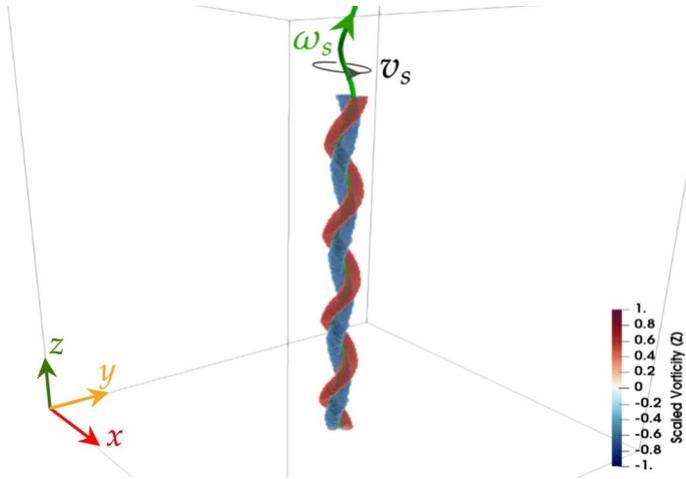
Fig. 1 Schematic diagram of a single helical superfluid vortex (green) and the normal fluid vorticity in the z-direction (red and blue for positive and negative vorticity values respectively). The normal fluid vorticity ω_z is normalised by the maximum value ω_{max}. Note how the normal fluid structures wrap around the superfluid vortex line as a double-helix (the 3D realisation of the normal fluid dipole described in the literature). The thickness of the superfluid vortex core (green) is exaggerated for visual purposes; in reality it is several orders of magnitude smaller than the normal fluid's structures shown in red and blue

energy, enstrophy and helicity [10–12] between the two fluids. The mutual friction therefore controls the generation of normal fluid and superfluid coherent structures [10, 13–16] (see Fig. 1), their possible coupling [17, 18], the spectral distribution of turbulent kinetic energy [18, 19], as well as the decay [20] and the dissipation of turbulent kinetic energy [21]. It is thus responsible for some of the observed similarities and differences between classical and quantum turbulence [1–4].

Our work focuses on this energy transfer between the two fluids. In all previous studies, this topic was investigated in the context of turbulence. In some studies the normal fluid was initially turbulent and drove the growth of a superfluid vortex tangle [18–20, 22]); in others, a superfluid vortex tangle excited an initially quiescent normal fluid [12, 23]. Unfortunately, the turbulent context, requiring a statistical interpretation, complicates the analysis of the results. In order to better capture the essential physics of the energy transfer, here we study the simpler dynamics (laminar rather than turbulent) of two vortex-antivortex pairs, with each vortex perturbed by a single, helical Kelvin wave. We consider two problems (see Fig. 2). In the first problem, the vortex lines with Kelvin waves are embedded in an initially quiescent normal fluid; in the second problem, they are in the presence of an imposed counterflow (a configuration which leads to the well-known Donnelly–Glaberson instability [24]). Similar vortex configurations, currently examined in ongoing experiments [16], are ubiquitous in turbulent flows, but they are simple enough that we can relate the temporal evolution of the geometry of
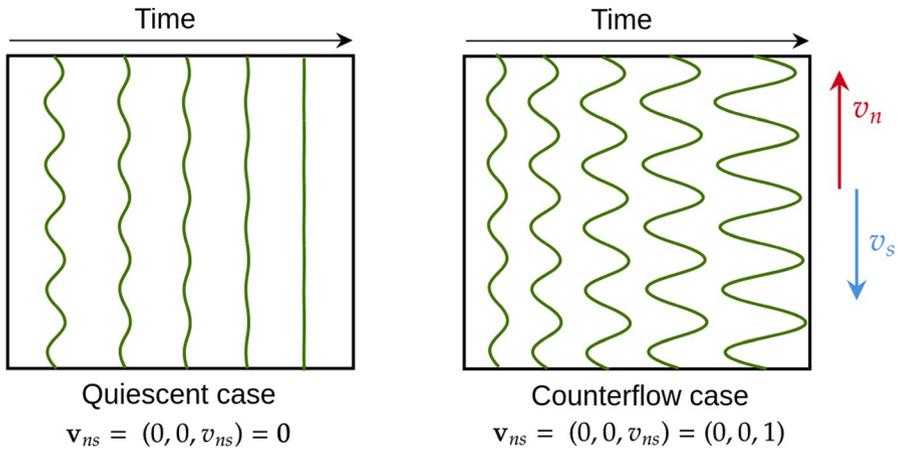
Fig. 2 Schematic time evolution of the Kelvin wave in the first problem (left: Kelvin wave in initially quiescent normal fluid) and in the second problem (right: Kelvin wave in the presence of counterflow)

the vortex line with the injection and the dissipation of energy in the normal fluid via the mutual friction force.

The study utilises a recent theoretical model capable of simulating self-consistently the coupled motion of normal fluid and superfluid [25]; in particular the model predicts quantitatively the experimentally observed shrinking of superfluid vortex rings [26].

The paper is organised as follows: Sect. 2 briefly describes the model and the parameters used in our simulations; Sect. 3 presents the results; Sect. 4 summarises the conclusions.

2 Method

The vortex core radius of superfluid ^{4}He ($a_0 \approx 10^{-8}$cm) is several orders of magnitudes smaller than any length scale of interest in turbulent flows. Following Schwarz [27], we hence describe vortex lines as space curves $\mathbf{s}(\xi, t)$ of infinitesimal thickness carrying one quantum of circulation $\kappa = h/m_4 = 9.97 \times 10^{-8}$ m^2/s, where h is Planck's constant, $m_4 = 6.65 \times 10^{-27}$kg is the mass of one helium atom, ξ is arclength and t is time. The equation of motion of the vortex line is

$$\dot{\mathbf{s}}(\xi, t) = \frac{\partial \mathbf{s}}{\partial t} = \mathbf{v}_{s_\perp} + \beta \mathbf{s}' \times (\mathbf{v}_n - \mathbf{v}_s) + \beta' \mathbf{s}' \times [\mathbf{s}' \times (\mathbf{v}_n - \mathbf{v}_s)] \ , \qquad (1)$$

where $\mathbf{s}' = \partial \mathbf{s}/\partial \xi$ is the unit tangent vector at $\mathbf{s}$, $\mathbf{v}_n$ and $\mathbf{v}_s$ are the normal fluid and superfluid velocities at $\mathbf{s}$, and β, β' are temperature and Reynolds number dependent mutual friction coefficients [25]. The $\mathbf{v}_{s_\perp}$ term indicates the projection of superfluid velocity on a plane orthogonal to $\mathbf{s}'$. The superfluid velocity at a point $\mathbf{x}$ induced by the entire vortex configuration $\mathcal{T}$ is determined by the Biot–Savart law:

$$\mathbf{v}_s(\mathbf{x}, t) = \frac{\kappa}{4\pi} \oint_{\mathcal{T}} \frac{\mathbf{s}'(\xi, t) \times [\mathbf{x} - \mathbf{s}(\xi, t)]}{|\mathbf{x} - \mathbf{s}(\xi, t)|^3} d\xi \quad . \tag{2}$$

Usually Eqs. (1) and (2) are always meant to be supplemented by a vortex reconnection algorithm [28]) to cope with collisions of vortex lines: In this study, such collisions do not occur. This model of vortex lines is valid under the condition that the discretisation on the lines $\Delta \xi$ is smaller than the average vortex distance ℓ and much greater than the vortex core radius a_0.

Evolving the vortex lines using Eqs. (1) and (2) gives rise to a *one-way model* that neglects the back reaction of the vortex lines onto the normal fluid. Accounting for this back reaction, however, is crucial to understand more accurately the interaction between the two fluids. A *two-way model* is obtained by evolving the normal fluid self-consistently [25] according to the Navier–Stokes equation for $\mathbf{v}_n$ modified by the introduction of the mutual friction force per unit volume $\mathbf{F}_{ns}$:

$$\frac{\partial \mathbf{v}_n}{\partial t} + (\mathbf{v}_n \cdot \nabla)\mathbf{v}_n = -\frac{1}{\rho} \nabla p + \nu_n \nabla^2 \mathbf{v}_n + \frac{\mathbf{F}_{ns}}{\rho_n} \tag{3}$$

$$\mathbf{F}_{ns} = \oint_{\mathcal{T}} \mathbf{f}_{ns}(\mathbf{s}) \delta(\mathbf{x} - \mathbf{s}) d\xi, \quad \nabla \cdot \mathbf{v}_n = 0 \tag{4}$$

where $\rho = \rho_n + \rho_s$ is the total helium density, ρ_n and ρ_s are, respectively, the normal and superfluid densities, p is the pressure, ν_n is the kinematic viscosity of the normal fluid and $\mathbf{f}_{ns}$ is the local friction per unit length [29], defined by

$$\mathbf{f}_{ns}(\mathbf{s}) = -D\mathbf{s}' \times \left[\mathbf{s}' \times (\dot{\mathbf{s}} - \mathbf{v}_n) \right] - \rho_n \kappa \mathbf{s}' \times (\mathbf{v}_n - \dot{\mathbf{s}}), \tag{5}$$

where the coefficient D is

$$D = \frac{4\pi \rho_n \nu_n}{\left[\frac{1}{2} - \gamma - \ln\left(\frac{|\mathbf{v}_{n_\perp} - \dot{\mathbf{s}}| a_0}{4\nu_n} \right) \right]}, \tag{6}$$

where here $\mathbf{v}_{n_\perp}$ represents the normal fluid velocity lying on a plane orthogonal to $\mathbf{s}'$, and $\gamma = 0.5772$ is the Euler–Mascheroni constant. The hydrodynamic model of the normal fluid is valid under the continuum approximation of the Navier–Stokes equations; this approximation is valid as the discretisation of the normal fluid grid Δx is larger than the roton-roton mean free path $\lambda_{mfp} = 3\nu_n/v_G$, where $v_G = \sqrt{2k_B T/(\pi \mu)}$ is the roton group velocity and $\mu = 0.16 m_4$ is the effective mass of a roton. The separation of these two length scales is in fact of several orders of magnitude $\Delta x/\lambda_{mfp} \sim 10^4$. Methods for fully-coupled dynamics have been used in recent studies [14, 15, 25, 29, 30]: the results presented here are based on [15, 29]. The counterflow velocity is forced in the normal fluid by imposing the 0-th Fourier mode in our spectral code, while in the superfluid component by imposing a constant background vector.

In this paper, we use the two-way model to solve the two problems described in Sect. 1. We solve the governing equations and report input parameters and results

using dimensionless units. We use a characteristic length scale $\tilde{\lambda} = D/L$, where $D^3 = (0.1\text{cm})^3$ is the dimensional cube size, $L^3 = (2\pi)^3$ is the size of the non-dimensional cubic computational domain and time scale $\tilde{\tau} = \tilde{\lambda}^2 v_n^0/v_n$, where v_n^0 is the dimensionless viscosity set to properly resolve the small scales of the normal fluid [25]. For this simulation, they are $\tilde{\lambda} = 1.59 \times 10^{-2}\text{cm}$, $v_n^0 = 0.04$ and $\tilde{\tau} = 4.58 \times 10^{-2}\text{s}$.

In both problems, we consider a $L^3 = (2\pi)^3$ cube with periodic boundary conditions at temperature $T = 1.9\text{K}$. Four helical vortex lines aligned in the z-direction with amplitude $A = 0.1$ and wavenumber $k = 5$ are initialised in a chess-board like configuration, such that each vortex (with anti-clockwise rotation) is exactly $L/2$ away from an anti-vortex (with clockwise rotation) and is left to evolve in time. This vortex configuration, unlike a single centralised vortex line, preserves a net-zero circulation under periodic boundary conditions. This one-vortex configuration could lead to inconsistencies due to boundary conditions not being satisfied. However due to the simple nature of the simulation, this effect is not significant. In the first problem the normal fluid is initially at rest, while in the second problem an imposed mean counterflow velocity $v_{ns} = 1$ in the z-direction fuels the Donnelly–Glaberson instability (see Figs. 1 and 2). The Lagrangian discretisation along the vortex lines has size $\delta = 0.02$ (corresponding to an initial number of vortex discretisation points equal to 1872) with timestep $\Delta t_{VF} = 6.25 \times 10^{-5}$. To solve Eq. (3) for the normal fluid we use an Eulerian discretisation with $N = 256^3$ mesh points and timestep $\Delta t_{NS} = 40\Delta t_{VF}$. The analysis of the results presented relate to a single vortex line, and global normal fluid quantities are computed across the quadrant in which the vortex resides.

3 Results

3.1 Kelvin Wave in Initially Quiescent Normal Fluid

The initial condition of the first problem consists of a Kelvin wave on a vortex line in an initially quiescent normal fluid. At small amplitudes, the Kelvin wave rotates with angular frequency $\omega \propto k^2$, neglecting logarithmic corrections. The relative motion between the vortex line and the normal fluid induces a mutual friction that creates a dipole pattern in the normal fluid around the vortex line, as previously reported in the literature for a single vortex ring [10], a single vortex line [11]) and a bundled vortex structure [15]. In our case the dipole pattern is twisted in a helical shape, as illustrated in Fig. 1. As the Kelvin wave propagates, it injects vorticity and energy into the normal fluid. Consequently the superfluid loses energy, corresponding to a decrease of the amplitude of the Kelvin wave. This decrease can clearly be observed in Fig. 3a (blue curves), where the numerically computed temporal evolution of the Kelvin wave's amplitude according to the two-way model is reported along with the prediction of the one-way model in the local induction approximation (LIA), which can be calculated
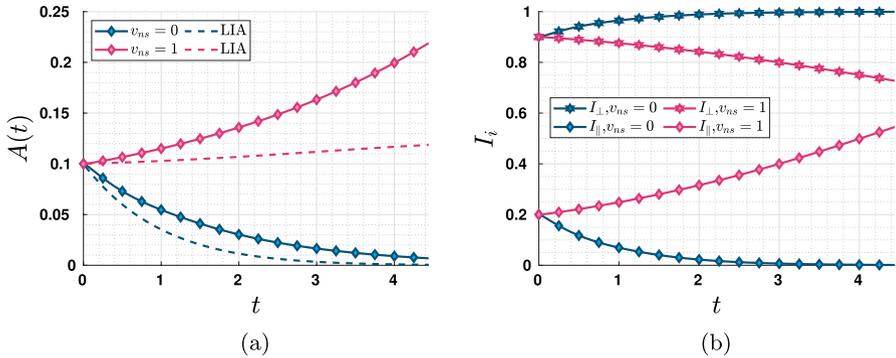
Fig. 3 *Left:* Evolution of the Kelvin wave's amplitude: comparison between two-way model (solid lines with red/blue symbols) and one-way model in the LIA (dashed lines). The blue symbols refer to the first problem (Kelvin wave in initially quiescent normal fluid), and the red symbols to the second problem (Kelvin wave in the presence of counterflow). *Right:* Anisotropic parameters $I_\parallel$ and $I_\perp$ computed using the two-way model corresponding to the first problem (blue symbols) and the second problem (red symbols)

analytically. We observe that the two-way coupled decay of the Kelvin wave is slower, prolonging the lifetime of the Kelvin wave. This effect has also been observed in recent numerical [15] and experimental [26] studies of vortex rings.

The decay of the Kelvin wave towards a straight vortex line can also be observed in Fig. 3b (blue curves) where we report the temporal evolution of the anisotropic parameters $I_\parallel$ and $I_\perp$ [31, 32]. The parameters quantify the anisotropy of the vortex configuration in the directions parallel and perpendicular to the counterflow direction, which are obtained by

$$I_\parallel = \frac{1}{\Omega L'} \oint_{\mathcal{T}} [1 - (\mathbf{s}' \cdot \hat{\mathbf{r}}_\parallel)^2] d\xi, \tag{7}$$

$$I_\perp = \frac{1}{\Omega L'} \oint_{\mathcal{T}} [1 - (\mathbf{s}' \cdot \hat{\mathbf{r}}_\perp)^2] d\xi, \tag{8}$$

where $\hat{\mathbf{r}}_\parallel$ is the unit vector parallel to the *z*-direction, $\hat{\mathbf{r}}_\perp$ is the unit vector parallel to the *x*-direction, L' is the vortex line density (vortex length per unit volume) defined by $L' = (1/\Omega) \oint_{\mathcal{T}} d\xi$, and Ω is the volume of the computational domain. The decay of the Kelvin wave into a straight vortex in fact implies that $I_\parallel \to 0$ and $I_\perp \to 1$.

The decaying amplitude $A(t)$ of the Kelvin wave also implies that the magnitude of the velocity difference $\dot{\mathbf{s}} - \mathbf{v}_n$ decreases with time, reducing the magnitude of the mutual friction $\mathbf{f}_{ns}$: this effect is reported in Fig. 4a. In the first approximation, in fact, we have $|\mathbf{f}_{ns}| \propto |\dot{\mathbf{s}} - \mathbf{v}_n| \approx |\dot{\mathbf{s}}| \propto \zeta \propto A$, where $\zeta = |\mathbf{s}''|$ is the curvature of the vortex line at $\mathbf{s}$.

To monitor the transfer of energy between the two fluids, we compute the energy injected per unit time by the superfluid vortex into the normal fluid, defined as
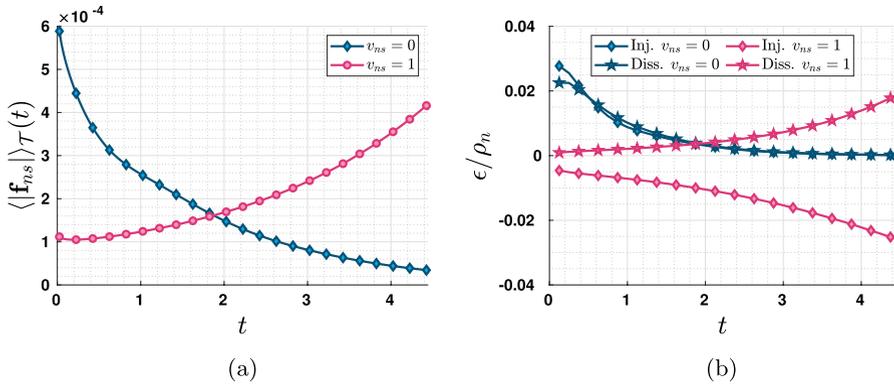
Fig. 4 Temporal evolution of the average mutual friction $\mathbf{f}_{ns}(\mathbf{s})$ (*left*) and of the injection/dissipation per unit mass of normal fluid (*right*). The blue symbols refer to the first problem (Kelvin wave in initially quiescent normal fluid) and the red symbols to the second problem Kelvin wave in the presence of counterflow). Note here that unlike the amplitude, $\mathbf{f}_{ns}$ in the quiescent case does not decay to 0, but rather a finite value. The vortices in the configuration do in fact move with a small but nonzero translational velocity induced by the other vortices, stirring the normal fluid

$$\epsilon_{inj} = \int_{\Omega} \mathbf{F}_{ns} \cdot \mathbf{v}_n d^3\mathbf{x} \ , \tag{9}$$

coinciding with the effective work per unit time performed by the mutual friction force on the normal fluid. This energy injection generates velocity gradients (i.e. vorticity, see Fig. 1) into the normal fluid, hence induces the viscous dissipation

$$\epsilon_{diss} = \nu_n \rho_n \int_{\Omega} \omega^2 d^3\mathbf{x} \ , \tag{10}$$

The temporal evolutions of ϵ_{inj} and ϵ_{diss} are reported in Fig. 4b, where we observe that the energy injected is rapidly dissipated by viscosity. In the initial transient phase, the injection of normal fluid energy dominates, until dissipation takes over.

3.2 Kelvin Wave in the Presence of Counterflow

In the second problem, we impose a background counterflow along the z axis; the average normal fluid velocity is in the positive z direction (hence parallel to the superfluid vorticity). Provided that $v_n > v_n^c$ where v_n^c is a critical velocity, the imposed normal flow feeds energy into the superfluid, hence the amplitude of the Kelvin wave grows (Donnelly–Glaberson instability). The critical velocity v_n^c can be determined analytically in the one-way model under constant $\mathbf{v}_n$ and the LIA. The resulting temporal evolution of the amplitude of the Kelvin wave is $A(t) = A_0 e^{\sigma t}$, where A_0 is the initial amplitude, $\sigma = \alpha k(v_{ns} - \gamma k)$ is the growth rate, $\gamma = \kappa/(4\pi)\ln(1/(\zeta a_0))$, α is the friction coefficient in the one-way model, and k the Kelvin wave's wavenumber. Hence, the Kelvin wave grows in amplitude if the amplitude of the imposed normal fluid is larger than $v_n^c = (\rho_s/\rho)(\kappa/(4\pi))k \ln(1/(\zeta a_0))$ [33]. If we choose $v_n > v_n^c$ then

the amplitude of the Kelvin wave grows, as shown in Fig. 3a (red curves). If we compare the growth rate of the two-way model with the one obtained analytically with LIA employing the one-fluid model, we obtain a substantial difference, as expected. In fact, LIA is a too simple framework to describe accurately the evolution of the Kelvin wave, neglecting the relevance of the logarithmic correction. In addition, LIA is a good approximation only if $A(t)k \ll 1$ and furthermore the friction coefficients of the two-way model are different from the coefficients of the original one-way model of Schwarz.

The growth of the Kelvin wave's amplitude with respect to time leads tangent vectors to the vortex line to progressively lie on a horizontal xy plane. For large times, the amplitude of the Kelvin wave becomes comparable to the wavelength, $A \simeq 2\pi/k$, and the behaviour of the helix becomes similar to that of stacked vortex rings. At large amplitude, the vortex effectively lies on the xy plane (orthogonal to the counterflow velocity $\mathbf{v}_{ns}$), such that in time $I_{\parallel} \to 1$ and $I_{\perp} \to 1/2$, as it can be observed in Figs. 3b and 5 (see Appendix A).

The increase of the angle between the counterflow direction and the tangents to the superfluid vortex is responsible for the observed stronger intensity of the mutual friction force as time increases, see Fig. 4a. The increasing magnitude of $|\mathbf{f}_{ns}|$ leads to an increase of $|\epsilon_{inj}|$ reported in Fig. 4b. The negative value of ϵ_{inj} confirms that the energy is globally transferred from the normal fluid to the superfluid vortex. As in the previous numerical experiment where the normal fluid is initially quiescent, the motion of the superfluid vortex lines injects vorticity in the normal fluid resulting in the onset of viscous dissipation. It is worth noting that compared to the quiescent case, the magnitudes of energy injection and dissipation exhibit a completely different character: both quantities do in fact increase with time.

4 Conclusion

We have studied the transfer of energy between normal fluid and superfluid numerically in two simple problems in which the motion of the fluids is laminar and the vortex configuration is simple. The main feature of our study is the use of a recently-developed two-way model [25] capable of accounting for experimental results reported in literature about mildly turbulent bundles of vortex rings [26, 34]. We have related the evolution of the geometry of the vortex line to the normal fluid energy injection and dissipation. In the first problem (a Kelvin wave propagating in a normal fluid background initially at rest) energy is transferred from the superfluid into the normal fluid and eventually dissipated into heat. In the second problem (a Kelvin wave in the presence of an imposed thermal counterflow) both energy injection and dissipation increase with time. When compared to analytical results obtained using the one-way Local Induction Approximation (LIA), in the counterflow case the self-consistent nature of the two-way model drives a significantly more rapid amplitude growth, while in the quiescent case, with respect to LIA, the Kelvin waves are less attenuated by motions induced in the normal fluid around the vortex line. The analytic derivation of LIA is based on the amplitude

being much smaller in comparison with the wavelength, an approximation which becomes invalid as the amplitude increases. As this occurs, the non-local interactions which are neglected in LIA become significant in the dynamics, and hence LIA is not a valid approximation. As expected, LIA is a too simplified model for the systems investigated in this work.

These results strengthen our understanding of two-fluid hydrodynamics, which will be soon tested in on-going experiments [16] on decay and amplification of Kelvin waves in a rotating cryostat.

Appendix

Extended Anistropic Parameters Figure

For consistency, the time duration of the plots in Figs. 3 and 4 was constrained to $t \sim 4.5$, such that the re-meshing [25] of vortex filaments did not factor into the analysis. In particular, the mutual friction in Fig. 4a is affected by the re-meshing algorithm, and therefore our analysis is only relevant in the duration up to the re-meshing of the vortex filaments in the counterflow case. Since the anisotropic parameters $I_{\parallel}$ and $I_{\perp}$ are dependent on the geometry of the vortex configuration only, they are not affected by the re-meshing algorithm (see Fig. 5).

In the counterflow case, as the amplitude of the Kelvin wave becomes sufficiently large $Ak >> 1$, the non-local interaction dominates the local interaction. The resulting configuration resembles a stack of k vortex rings. A vortex ring of radius R can be parameterised by the arclength ξ to give $\mathbf{s}(\xi) = (R\cos(\xi/R), R\sin(\xi/R), z)$. The parallel anisotropic parameter gives $I_{\parallel} = 1$, while the perpendicular gives

$$I_{\perp} = \frac{1}{\Omega L'} \int_0^{2\pi R} 1 - (\mathbf{s}' \cdot r_{\perp})^2 d\xi = \frac{1}{2\pi R} \int_0^{2\pi R} \cos^2(\xi/R) d\xi = \frac{1}{2}. \tag{11}$$

In the later stages of Fig. 5, it can be seen that the parameters in the counterflow case begin to asymptote to the values as calculated for a single vortex ring. This confirms the geometry of the vortex configuration, resembling stacked vortex rings.

Fig. 5 The full time evolution of the parameters $I_{\parallel}$ and $I_{\perp}$
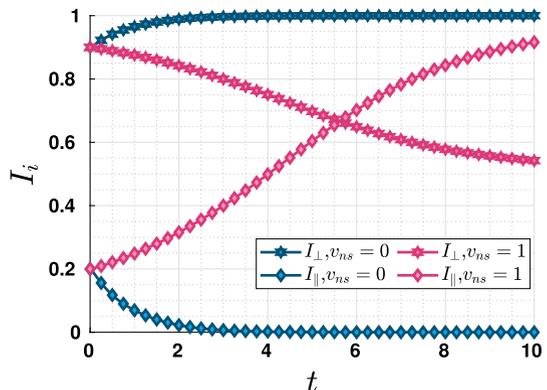
Author Contributions PZS performed the numerical simulations and created Fig. 1, 2, 3, 4. LG, GK and AWB wrote the code used in simulations. All authors participated in the writing and reviewing of the manuscript.

Declarations

Conflict of interest The authors declare no competing interests.

References

1. W. Vinen, J. Niemela, Quantum turbulence. J. Low Temp. Phys. **128**, 167 (2002)
2. L. Skrbek, K. Sreenivasan, Developed quantum turbulence and its decay. Phys. Fluids **24**, 011301 (2012)
3. C. Barenghi, L. Skrbek, K. Sreenivasan, Introduction to quantum turbulence. Proc. Natl. Acad. Sci. U.S.A. **111**(1), 1–4647 (2014)
4. C. Barenghi, H. Middleton-Spencer, L. Galantucci, N. Parker, Types of quantum turbulence. AVS Quantum Sci. **5**, 025601 (2023)
5. R. Feynmann, II. Application of quantum mechanics to liquid helium, vol. 1, C.J. Gorter edn. North Holland, Amsterdam, p. 36 (1955)
6. L. Onsager, Statistical hydrodynamics. Nuovo Cim **6**(Suppl. 2), 249 (1949)
7. H.E. Hall, W.F. Vinen, The rotation of liquid helium ii. i. Experiments on the propagation of secound sound in uniformly rotating helium ii. Proc. R. Soc. London A **238**(1213), 204 (1956)
8. L. Tisza, Transport phenomena in helium ii. Nature **141**, 913 (1938)
9. L.D. Landau, Theory of the superfluidity of helium ii. J. Phys. USSR **5**, 71 (1941)
10. D. Kivotides, C. Barenghi, D. Samuels, Triple vortex ring structure in superfluid helium ii. Science **290**, 777 (2000)
11. O.C. Idowu, A. Willis, C.F. Barenghi, D.C. Samuels, Local normal-fluid helium ii flow due to mutual friction interaction with the superfluid. Phys. Rev. B **62**, 3409 (2000)
12. D. Kivotides, Turbulence without inertia in thermally excited superfluids. Phys. Lett. A **341**, 193 (2005)
13. D. Kivotides, Interactions between normal-fluid and superfluid vortex rings in helium-4. EPL **112**, 36005 (2015)
14. D. Kivotides, Superfluid helium-4 hydrodynamics with discrete topological defects. Phys. Rev. Fluids **3**(10), 104701 (2018)
15. L. Galantucci, G. Krstulovic, C.F. Barenghi, Friction-enhanced lifetime of bundled quantum vortices. Phys. Rev. Fluids **8**(1), 014702 (2023)
16. C. Peretti, J. Vessaire, M. Gibert. Durozoy, Direct visualization of the quantum vortex lattice structure, oscillations, and destabilization in rotating ^{4}He. Sci. Adv. **9**(30), 2899 (2023)

17. K. Morris, J. Koplik, D. Rouson, Vortex locking in direct numerical simulations of quantum turbulence. Phys. Rev. Lett. **101**, 015301 (2008)
18. D. Kivotides, Spreading of superfluid vorticity clouds in normal-fluid turbulence. J. Fluid Mech. **668**, 58 (2011)
19. D. Kivotides, Energy spectra of finite temperature superfluid helium-4 turbulence. Phys. Fluids **26**, 105105 (2014)
20. D. Kivotides, Decay of finite temperature superfluid helium-4 turbulence. J. Low Temp. Phys. **181**, 68 (2015)
21. L. Galantucci, E. Rickinson, A.W. Baggaley, N.G. Parker, C.F. Barenghi, Dissipation anomaly in a turbulent quantum fluid. Phys. Rev. Fluids **8**(3), 034605 (2023)
22. D. Kivotides, Coherent structure formation in turbulent thermal superfluids. Phys. Rev. Lett. **96**, 175301 (2006)
23. D. Kivotides, Relaxation of superfluid vortex bundles via energy transfer to the normal fluid. Phys. Rev. B **76**, 054503 (2007)
24. W.I. Glaberson, W.W. Johnson, R.M. Ostermeier, Instability of a vortex array in he ii. Phys. Rev. Lett. **33**(20), 1197 (1974)
25. L. Galantucci, A.W. Baggaley, C.F. Barenghi, G. Krstulovic, A new self-consistent approach of quantum turbulence in superfluid helium. Eur. Phys. J. Plus **135**(7), 1–28 (2020)
26. Y. Tang, W. Guo, H. Kobayashi, S. Yui, M. Tsubota, T. Kanai, Imaging quantized vortex rings in superfluid helium to evaluate quantum dissipation. Nature Comm. **14**(1), 2941 (2023)
27. K. Schwarz, Three-dimensional vortex dynamics in superfluid ^{4}He. Phys. Rev. B **38**(4), 2398 (1988)
28. A.W. Baggaley, The sensitivity of the vortex filament method to different reconnection models. J. Low Temp. Phys. **168**(1–2), 18–30 (2012)
29. L. Galantucci, M. Sciacca, C.F. Barenghi, Coupled normal fluid and superfluid profiles of turbulent helium ii in channels. Phys. Rev. B **92**(17), 174530 (2015)
30. S. Yui, H. Kobayashi, M. Tsubota, W. Guo, Fully coupled two-fluid dynamics in superfluid he 4: anomalous anisotropic velocity fluctuations in counterflow. Phys. Rev. Lett. **124**(15), 155301 (2020)
31. K. Schwarz, Three-dimensional vortex dynamics in superfluid ^{4}He: homogeneous superfluid turbulence. Phys. Rev. B **38**(4), 2398 (1988)
32. H. Adachi, S. Fujiyama, M. Tsubota, Steady-state counterflow quantum turbulence: simulation of vortex filaments using the full biot-savart law. Phys. Rev. B **81**(10), 104511 (2010)
33. M. Tsubota, C.F. Barenghi, T. Araki, A. Mitani, Instability of vortex array and transitions to turbulence in rotating helium ii. Phys. Rev. B **69**(13), 134515 (2004)
34. H. Borner, T. Schmeling, D. Schmidt, Experiments on the circulation and propagation of largescale vortex rings in heii. Phys. Fluids **26**, 1410 (1983)

Authors and Affiliations

Piotr Z. Stasiak[1] · Andrew W. Baggaley[1] · Giorgio Krstulovic[2] · Carlo F. Barenghi[1] · Luca Galantucci[1,3]

✉ Piotr Z. Stasiak
 p.stasiak@newcastle.ac.uk

 Andrew W. Baggaley
 a.baggaley@newcastle.ac.uk

 Giorgio Krstulovic
 giorgio.krstulovic@oca.eu

Carlo F. Barenghi
c.barenghi@newcastle.ac.uk

Luca Galantucci
l.galantucci@iac.cnr.it

1   School of Mathematics, Statistics and Physics, Newcastle University, Newcastle Upon Tyne NE1 7RU, UK

2   Laboratoire Lagrangre, Université Côte d'Azur, Observatoire de la Côte d'Azur, CNRS, Boulevard de l'Observatoire CS 34229, 06304 Nice Cedex 4, France

3   Istituto per le Applicazioni del Calcolo M. Picone, IAC-CNR, Via dei Taurini 19, 00185 Roma, Italy